New sol–gel synthesis of a $(CaO)_{0.3}(Na_2O)_{0.2}(P_2O_5)_{0.5}$ bioresorbable glass and its structural characterisation

David M. Pickup,*[a] Paul Guerry,[b] Robert M. Moss,[a] Jonathan C. Knowles,[c] Mark E. Smith[b] and Robert J. Newport[a]

Received 2nd July 2007, Accepted 17th September 2007
First published as an Advance Article on the web 25th September 2007
DOI: 10.1039/b709955j

An improved sol–gel synthesis of $(CaO)_{0.3}(Na_2O)_{0.2}(P_2O_5)_{0.5}$ bioresorbable glass has been developed. The structures of both the dried gel and the stabilised sol–gel glass have been characterised using high-energy XRD, ^{31}P MAS NMR and FT-IR spectroscopy. The structure of the analogous melt-quench prepared glass has also been studied for comparison. The results show that the dried gel has a structure consisting of mainly Q^0 and Q^1 phosphate units, whereas that of the stabilised sol–gel glass comprises predominantly Q^1 and Q^2 units. Furthermore, it is demonstrated that the structure of the sol–gel glass is similar to that of its melt-quenched counterpart except for the presence of hydroxyl groups which terminate the phosphate chains, reducing the connectivity of the network.

Introduction

A current trend in biomaterials development is a move from passive, inert implant materials to those that degrade and play an active part in the regeneration of tissue.[1] Implant materials are now being designed with the aim of promoting a specific biological response within the human body. This new class of materials is often referred to as the 'Third Generation' of biomaterials, and included in this class are phosphate-based glasses.

Phosphate glasses have a number of properties which lend them to potential applications in the field of biomaterials.[1] Phosphate-based glasses containing ions routinely found in the human body (such as Ca^{2+} and Na^+) can be classed as bioresorbable and biocompatible. They have predictable dissolution rates which can be controlled by varying the composition, and being entirely amorphous, the dissolution is relatively uniform and there is little risk of residual fragments causing sterile inflammation. Melt-quenched glasses in the ternary system $CaO–Na_2O–P_2O_5$ with a high CaO content (>24 mol%) and low dissolution rate show excellent *in vitro* biocompatibility with a significant increase in cell proliferation relative to the control.[2] There has been significant interest in these glasses when manufactured as fibres for potential use in tissue engineering, and in particular for any tissue with a medium to high anisotropy, such as muscle and ligament.[3,4] Other potential clinical applications of phosphate-based glasses include as bacterial control devices *via* the incorporation of antimicrobial ions such as silver,[5,6] as neural repair devices when manufactured in a tubular form[7,8] and as a component in oral healthcare products when doped with fluoride ions.[9,10]

[a]*School of Physical Sciences, University of Kent, Canterbury, UK CT2 7NH*
[b]*Department of Physics, University of Warwick, Coventry, UK CV4 7AL*
[c]*Division of Biomaterials and Tissue Engineering, UCL Eastman Dental Institute, 256 Gray's Inn Road, London, UK WC1X 8LD*

Preparing $CaO–Na_2O–P_2O_5$ glasses by a sol–gel method offers some significant advantages over conventional melt-quenching techniques. Firstly, glassy films can be prepared which allows scope for devices to be coated with a biocompatible layer, and secondly, the processing can be modified to produce porous materials, which is important in tissue engineering where meso- and macrostructure are vital in terms of cell growth and nutrient supply to regenerated tissue. The low temperature nature of the sol–gel route also offers potential for the inclusion of biocompatible polymers in the synthesis to produce composite materials with improved mechanical properties and for the incorporation of active molecules such as antibiotics, growth factors and for the delivery of DNA.

The preparation of phosphate-based glasses by sol–gel methods is significantly more demanding than the preparation of silicate glasses by the same methods: the hydrolysis of alkyl phosphates is very slow under sol–gel conditions and phosphate anions (*e.g.* PO_4^{3-}) tend to form precipitates rather than network structures based upon P–O–P bonding.[11] To date, the most successful sol–gel method for the preparation of $CaO–Na_2O–P_2O_5$ glasses is based upon the reaction of mono- and di-substituted ethyl phosphate with reactive alkoxides of calcium and sodium.[12] This method, however, has significant disadvantages in that relatively high temperatures are required to remove the ethylene glycol solvent from the gels and the resultant glasses do not exhibit significant porosity, possibly as a result of the necessary heat treatment. Recently, we have developed a new sol–gel route to phosphate-based materials that produces glassy gels at lower temperatures than previously reported. Furthermore, this method can be used to produce porous foams, which have potential applications as tissue engineering scaffolds.

Here we report the structural characterisation of $CaO–Na_2O–P_2O_5$ sol–gel glass prepared by the new method. We have used a combination of high-energy X-ray diffraction (HEXRD), ^{31}P magic angle spinning (MAS) and ^{1}H–^{31}P

cross-polarisation (CP) MAS NMR, and FT-IR spectroscopy to understand the structure of the new materials and how this relates to the structure of the analogous melt-quenched glass. Further characterisation of the samples was provided by thermal analysis, high-temperature X-ray diffraction (HTXRD) and ^{1}H–^{13}C CP MAS NMR. The nominal composition of $(CaO)_{0.3}(Na_2O)_{0.2}(P_2O_5)_{0.5}$ was chosen because the melt-quenched glass of this composition exhibits good biocompatibility and can be readily drawn into fibres.[13] This composition has formed the basis of a number of studies involving the partial substitution of Na_2O for another metal oxide to improve the properties, *e.g.* Fe_2O_3 to improve the chemical durability of fibres designed to transplant muscle precursor cells as a treatment for muscle diseases and CuO to impart antimicrobial properties.[14]

Experimental

Sample preparation

The following precursors were used, without further purification, in the sol–gel preparation: 1 : 1 molar mixture of mono- and di-substituted n-butyl phosphate ($OP(OH)_2(OBu^n)$ and $OP(OH)(OBu^n)_2$, Alfa Aesar, ~98%), sodium methoxide solution (NaOMe, Aldrich, 30 wt% in methanol) and calcium methoxyethoxide solution (Ca-methoxyethoxide, ABCR, 20 wt% in methoxyethanol).

The sol–gel preparation is outlined by the flowchart in Fig. 1. The n-butyl phosphate was first added dropwise using a syringe through a septum to a vessel containing the NaOMe solution: the solution was stirred magnetically throughout this addition. After one hour, the Ca-methoxyethoxide solution was added using the same method. The sol was then allowed to gel, which typically took ~2 h, and left overnight. During this

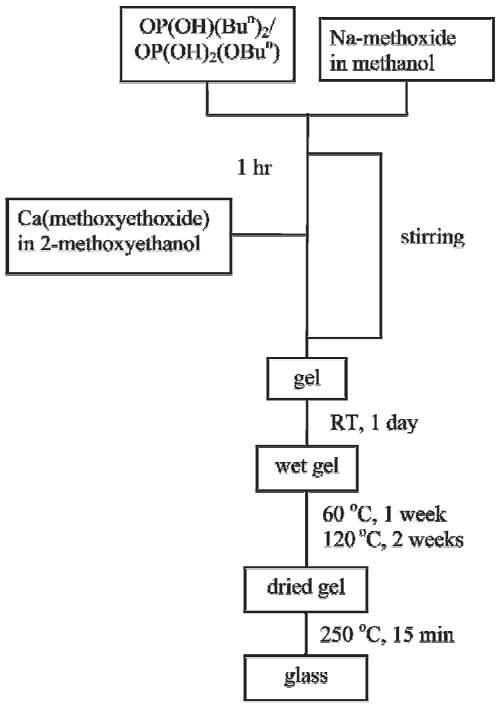

Fig. 1 Flow diagram of the sol–gel preparation.

period the gel liquefied, allowing the resultant sol to be cast in a polypropylene container. This sol was aged at 60 °C for one week, during which time the final gelation occurred, before drying at 120 °C for two weeks. This rather strange gelation behaviour is probably the result of the formation of solid oligomeric alkoxide intermediates during the early stage of the reaction, which later slowly dissolve in the solvent. The final gelation is the result of polymerisation of the phosphate groups which is known to be slow.[11] Half of the dried gel was heated to 250 °C to remove solvent, water and organic molecules. This calcination temperature was chosen on the basis of a thermogravimetric measurement (see later), which showed that the organic material remaining in the sample is driven off at ~250 °C.

The analogous melt-quenched glass sample was prepared using sodium dihydrogen orthophosphate (NaH_2PO_4, BDH, 99%), calcium carbonate ($CaCO_3$, BDH, 99+%) and phosphorus pentoxide (P_2O_5, BDH, 97%). The precursors were weighed out, mixed, placed in a Pt–10% Rh crucible (Type 71040, Johnson Matthey) and loaded into a preheated furnace (Carbolite, RHF 1500). The mixture was left at 300 °C for half an hour, raised to 600 °C for a further half an hour and finally melted at 1100 °C for one hour. The molten glass was then quenched by pouring onto a heavy steel plate.

Characterisation necessary for a quantitative analysis of the X-ray diffraction data was performed: elemental analysis (ICP-AES and gravimetric) was carried out by a commercial company (Medac Ltd) and macroscopic densities were determined by helium pycnometry using a Quantachrome Multipycnometer. The elemental analysis revealed that the composition of the oxide components of all the samples was within ±3 mol% of the nominal composition. As expected, the sol–gel samples contained some residual carbon and hydrogen: the dried gel contained 6.1 wt% C and 2.1 wt% H, whereas the sample calcined at 250 °C contained 1.7 wt% C and 0.4 wt% H.

Thermal analysis

Simultaneous thermogravimetric and differential thermal analysis of the sol–gel sample was carried out on a Setaram Labsys™ TG-DTA16 instrument. A heating rate of 20 °C min^{-1} to 1000 °C was used with a purge gas of nitrogen. The data were baseline-corrected using a blank run.

FT-IR spectroscopy

Infrared spectra were recorded in transmission mode on a Biorad FTS175C spectrometer controlled by Win-IR software. Samples were diluted in dry KBr and scanned in the range 4000–400 cm^{-1}. Each spectrum was the result of summing 64 scans.

High-temperature X-ray diffraction (HTXRD)

The HTXRD was measured on a Bruker D8 Advance diffractometer equipped with a LynxEye detector and an Anton Paar HTK1600 heating stage fitted with a Pt electrode. XRD patterns were collected from 2θ = 15 to 30° with a step of 0.02° and counting time of 19 s per point using Ni-filtered Cu Kα radiation generated at 35 kV and 45 mA. Data were

collected between 40 and 1000 °C at intervals of 10 °C using air as a purge gas. The heating rate between temperature points was 6 °C s^{-1}.

MAS NMR

The ^{31}P single-pulse MAS NMR experiments were carried out on a CMX Infinity spectrometer attached to an 8.45 T magnet giving a ^{31}P Larmor frequency of 145.77 MHz. Samples were placed in the magnet using a Doty 4 mm MAS probe and spun at 10–12 kHz. The Spinsight software was used to run experiments with a 2.7 μs pulse length corresponding to a π/6 tip angle with a pre-acquisition delay of 10 μs. A 20 s repetition time was used and no saturation was observed. Typically, 150 scans were accumulated to obtain a good signal to noise ratio. Solid $NH_4H_2PO_4$ was used as a secondary reference at 0.9 ppm such that the shifts reported here are given relative to the primary reference of 85% phosphoric acid (0 ppm).

The CP MAS experiments were carried out on a CMX Infinity+ spectrometer attached to a 7.05 T magnet. The Larmor frequencies for ^{13}C, ^{31}P, and ^{1}H were 75.47, 121.50, and 300.14 MHz, respectively. A Bruker 4 mm MAS probe was used and the samples spun at 12 kHz. For the proton channel, 100 kHz power was applied in order to obtain a 2.5 μs 90° pulse as well as effective decoupling during the acquisition period of 10.24 ms and 40 ms for ^{31}P and ^{13}C experiments, respectively. For both nuclei, 128 transients were accumulated with a repetition time of 3 s and a pre-acquisition delay of 60 μs. Optimal contact times were 3.5 ms for ^{13}C and 1 ms for ^{31}P. The ^{13}C spectra were referenced to the 20.5 ppm resonance from alanine (relative to tetramethylsilane at 0 ppm), whereas the ^{31}P spectrum was referenced to the 0.9 ppm resonance from $NH_4H_2PO_4$.

High-energy X-ray diffraction (HEXRD)

The HEXRD data were collected on Station 9.1 at the Synchrotron Radiation Source (SRS), Daresbury Laboratory, UK. The finely powdered samples were enclosed inside a 0.5 mm thick circular metal annulus by kapton windows and mounted onto a flat-plate instrumental set-up. The wavelength was set at $\lambda = 0.5092$ Å and calibrated using the K-edge of a Pd foil; this value was low enough to provide data to a high value of momentum transfer ($Q_{max} = 4\pi\sin\theta/\lambda \sim 22$ Å^{-1}). The data were reduced using a suite of programs written in-house: the initial stage of analysis of XRD data from an amorphous material involves the removal of background scattering, normalization, correction for absorption and subtraction of the self-scattering term.[15] No correction was made to account for multiple scattering since it may be neglected in high energy X-ray diffraction from thin samples such as these, given the relatively low sample attenuation.[16] The resultant scattered intensity, $i(Q)$, can reveal structural information by Fourier transformation to obtain the pair-distribution function:

$$T(r) = T^0(r) + \int_0^\infty Qi(Q)M(Q)\sin(Qr)\mathrm{d}(Q) \qquad (1)$$

where $T^0(r) = 2\pi^2 r\rho_o$ (r is the atomic separation between atoms and ρ_o is the macroscopic number density) and $M(Q)$ is a window function necessitated by the finite maximum experimentally attainable value of Q.

Structural information can be obtained from the diffraction data by modelling the Q-space data and converting the results to r-space by Fourier transformation to allow comparison with the experimentally determined correlation function.[17] The structural parameters used to generate the Q-space simulation are varied to optimise the fit to the experimental data. The Q-space simulation is generated using the following equation:

$$p(Q)_{ij} = \frac{N_{ij}w_{ij}}{c_j}\frac{\sin QR_{ij}}{QR_{ij}}\exp\left[\frac{-Q^2\sigma_{ij}^2}{2}\right] \qquad (2)$$

where $p(Q)_{ij}$ is the pair function in reciprocal space, N_{ij}, R_{ij} and σ_{ij} are the coordination number, atomic separation and disorder parameter, respectively, of atom i with respect to j, c_j is the concentration of atom j and w_{ij} is the weighting factor. The weighting factors are given by:

$$w_{ij} = \frac{2c_ic_jf(Q)_if(Q)_j}{\overline{f(Q)}^2} \text{ if } i \neq j \qquad (3)$$

or,

$$w_{ij} = \frac{c_i^2f(Q)_i^2}{\overline{f(Q)}^2} \text{ if } i = j \qquad (4)$$

where $f(Q)$ represents the Q-dependent X-ray form factors.

The errors associated with the HEXRD data arise mainly from the fitting process due to the problem of overlapping correlation shells. They have been estimated on the basis of the tolerance that a particular parameter may have without significantly changing the overall quality-of-fit. Some additional systematic error may occur from the data reduction process as a result of the approximations subsumed into the various data corrections (*e.g.* for Compton scattering), but past analysis of test-sample data, and data collected at different wavelengths, suggest that these errors are small compared to those arising from the numerical modelling of the experimental data.

Results and discussion

Sol–gel processing

Fig. 2 shows the combined TGA/DTA (thermogravimetric analysis/differential thermal analysis) trace obtained from the thermal analysis of the dried $(CaO)_{0.3}(Na_2O)_{0.2}(P_2O_5)_{0.5}$ sol–gel sample. Note that the small rise at the beginning of the TG trace is due to a slight mismatch with the blank background run which shows up as an increase in weight when subtracted from the actual data. The TGA trace exhibits two regions of significant mass loss: a sharp decrease in mass between 200–400 °C, and a gradual loss starting at about 600 °C. The sharp mass loss is most likely due to the loss of hydroxyls and unreacted alkoxide groups as consolidation of the sol–gel network structure occurs. This assignment is supported by a broad endothermic peak in the DTA trace centred at 275 °C which is consistent with the consumption of heat energy to decompose the alkoxide groups and drive off

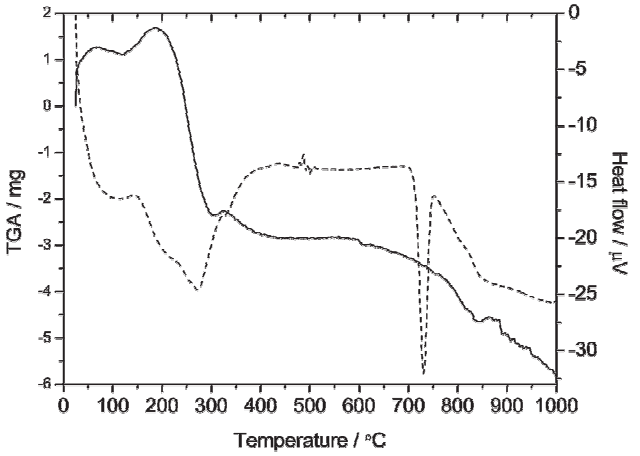

Fig. 2 Simultaneous TGA (solid line) and DTA (dashed line) measurements from the $(CaO)_{0.3}(Na_2O)_{0.2}(P_2O_5)_{0.5}$ sol–gel sample.

–OH groups. The second region of mass loss corresponds to a sharp endothermic peak in the DTA trace at 730 °C. This endothermic peak is probably associated with the densification of the material *via* the loss of micropores and increased network connectivity, and the decrease in mass due to the further loss of –OH groups as this occurs.

Fig. 3 shows the HTXRD data from the same sample along with the DTA trace which has been overlaid to allow some features in the XRD data to be correlated with thermal events. The onset of crystallisation can clearly be observed in the HTXRD data at ~470 °C. The appearance of Bragg peaks in the HTXRD data is accompanied by four sharp peaks in the DTA curve (two exothermic at 479 and 487 °C and two endothermic at 492 and 500 °C). The Bragg peaks in the HTXRD data continue to grow with temperature until 725 °C at which point the peaks at 2θ = 17.4, 26.9 and 28.6° all shift to lower angles and a new peak appears at 28.9°. The new Bragg peak grows in intensity very rapidly as a function of temperature. These changes in the XRD pattern suggest a

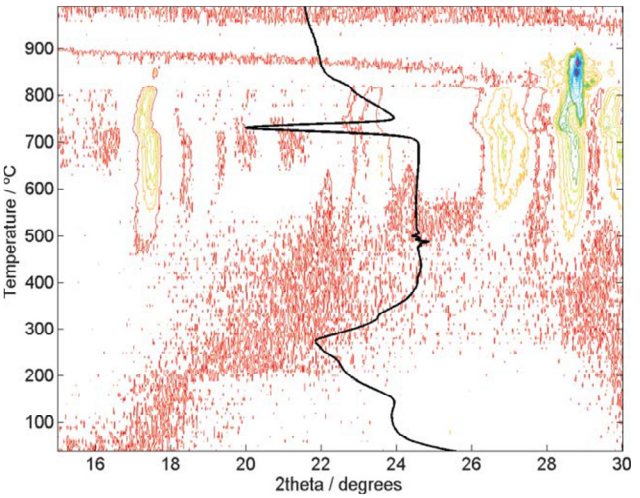

Fig. 3 HTXRD data from the $(CaO)_{0.3}(Na_2O)_{0.2}(P_2O_5)_{0.5}$ sol–gel sample. The solid black line is the DTA trace from Fig. 2 that has been overlaid to illustrate correlations between features in the two sets of data.

second crystallisation event and correlate very well with the sharp endothermic peak in the DTA trace at 730 °C. The fact that the peak in the DTA trace associated with the second crystallisation event is so much larger than that associated with the onset of crystallisation may indicate that phase separation is occurring with crystallisation of a minority phase at ~470 °C followed by bulk crystallisation at 730 °C. Although further measurements would be required to confirm this, the important result in the context of this work is that the combined DTA/HTXRD results accurately map the thermal stability of the sol–gel material. At 900 °C, all the Bragg peaks disappear indicating that the sample has melted.

The TGA/DTA and HTXRD data described above are invaluable when deciding upon the necessary heat treatment of the dried gel. The aim is to produce a stable product with as much of the residual organic components removed as possible. On the basis of the results described above, a calcination temperature of 250 °C was chosen because it lies beyond the temperature at which the structure starts to consolidate and yet well below the onset of crystallisation.

The presence of residual organic fragments in the dried gel and their removal by heat treatment was confirmed by ^{1}H–^{13}C CP MAS NMR. There are five sharp peaks in the spectrum from the dried gel (not shown), whereas for the gel heated to 250 °C no ^{1}H–^{13}C CP NMR signal could be detected. This removal of organic groups by heat treatment is consistent with the large weight loss shown in the TGA between 200 °C and 400 °C. Similar behaviour has previously been observed in silicate-based sol–gel materials.[18] The fact that no ^{1}H–^{13}C CP NMR signal could be detected from the heat-treated sol–gel sample despite the elemental analysis showing the presence of 1.7 wt% C suggests that this carbon is not hydrogenated and is probably present as a separate phase.

Structural characterisation

The structures of phosphate glasses are known to comprise PO_4^{3-} tetrahedra connected by between 1 and 3 bridging oxygen atoms (BOs) to form a network.[19] The connectivity of this phosphate network is commonly described by Q^n notation, where n refers the number of BOs in the PO_4^{3-} group. Thus a Q^3 PO_4^{3-} unit has 3 BOs to other PO_4^{3-} groups and one non-bridging oxygen (NBO), whereas a Q^0 PO_4^{3-} unit has 4 NBOs and is unconnected to other PO_4^{3-} tetrahedra. This connectivity is affected by the glass composition. Vitreous P_2O_5 has a structure composed entirely of Q^3 units; whereas the addition of metal oxides to phosphate glasses reduces this connectivity and introduces Q^1 and Q^2 groups into the structure. In such cases, the fractions of the various Q^n species can be estimated on the basis of glass composition, $(M_{2/v}O)_x(P_2O_5)_{1-x}$.[19] The $(CaO)_{0.3}(Na_2O)_{0.2}(P_2O_5)_{0.5}$ samples studied here are close to the metaphosphate composition (*i.e.* x = 0.5) and as such are expected to have structures composed entirely of Q^2 species.

Phosphorus NMR provides a method for measuring the relative quantities of the various Q^n species that comprise the glass structure. Fig. 4 shows ^{31}P MAS NMR spectra from the $(CaO)_{0.3}(Na_2O)_{0.2}(P_2O_5)_{0.5}$ samples and the ^{1}H–^{31}P CP MAS NMR spectrum from the stabilised sol–gel glass. Also

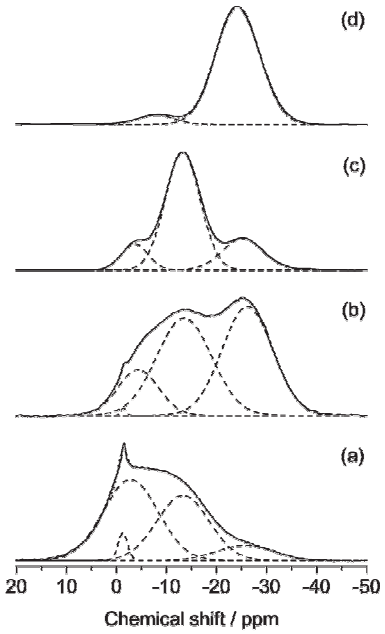

Fig. 4 ^{31}P MAS NMR spectra from the $(CaO)_{0.3}(Na_2O)_{0.2}(P_2O_5)_{0.5}$ samples showing the Gaussian deconvolution of the various resonances present: (a) dried gel, (b) stabilised sol–gel glass, (c) ^{1}H–^{31}P CP spectrum from the stabilised sol–gel glass and (d) melt-quenched glass.

shown is the Gaussian deconvolution of the various resonances present; the results of which are given in Table 1, along with the assignments of the resonances. The resonances at about −4, −13 and −26 ppm are assigned to Q^0, Q^1 and Q^2 species, respectively, according to a previous ^{31}P NMR study of $(CaO)_{0.5-x}(Na_2O)_x(P_2O_5)_{0.5}$ melt-quenched glasses.[20] The narrow resonance at close to −1 ppm is assigned to unreacted monomeric phosphates (*e.g.* $OP(OH)_{3-x}(OBu^n)_x$)[21] and given the label $Q^{0\prime}$ to distinguish it from the other orthophosphate Q^0 resonance: the narrowness of this resonance suggests that these monomeric phosphates are either more ordered in this sample or partially mobile. The results in Table 1 show the effect that the heat treatment has on the structure of the sol–gel. The dried gel has a structure dominated by Q^0 and Q^1 groups, whereas that of the stabilised sol–gel glass is composed of mainly Q^1 and Q^2 species. This is better illustrated by the average P–O–P coordination number ($N_{P\cdots P}$) which can be

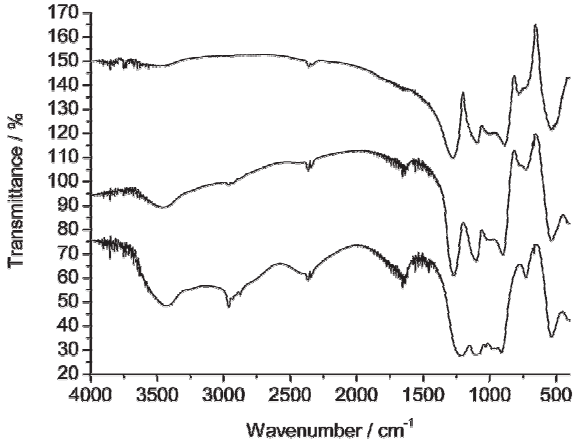

Fig. 5 FTIR spectra from the $(CaO)_{0.3}(Na_2O)_{0.2}(P_2O_5)_{0.5}$ samples: dried sol–gel (lower curve), stabilised sol–gel glass (middle curve) and melt-quenched glass (upper curve).

calculated from the Q^n speciation using the equation $N_{P\cdots P} = f_Q{}^1 + 2f_Q{}^2$ where $f_Q{}^n$ refers to the fraction of each Q^n group. Utilizing this approach, we arrive at a P–O–P coordination number of 0.6 ± 0.3 for the dried gel and 1.3 ± 0.2 for the stabilised sol–gel glass. This increase in $N_{P\cdots P}$ represents an increase in the connectivity between the phosphate groups with heat treatment, indicative of the structural evolution from a soft gel material to a stable glassy material. The ^{31}P CP MAS NMR spectrum shows an increase in intensity of the Q^0 and Q^1 resonances relative to the Q^2 resonance suggesting that the lower Q species are more strongly associated with protons. Considering this result alongside the ^{13}C CP MAS NMR results described earlier, we conclude that the reduced connectivity in the dried gel is associated with organic fragments and hydroxyl groups, whilst that in the stabilised sol–gel glass is associated only with hydroxyl groups. As expected, the ^{31}P NMR spectrum from the melt-quenched glass is dominated by the Q^2 resonance (95%) with a small peak due to Q^1 species, resulting in a P–O–P coordination number of 2.0 ± 0.2.

Further information on the nature of the bonding in the sol–gel samples can be gained from vibrational spectroscopy. Fig. 5 shows the FT-IR spectra from the dried gel and stabilised glass together with that from the melt-quenched sample for comparison. The absorption bands are assigned

Table 1 Results of the deconvolution of the ^{31}P MAS NMR spectra from the $(CaO)_{0.3}(Na_2O)_{0.2}(P_2O_5)$ sol–gel and melt-quenched samples using Gaussian functions

Sample	Assignment	Chemical shift (ppm) ±1.0 ppm	Width (ppm) ±2.0 ppm	Relative intensity (%) ±5.0%
Dried gel (120 °C)	$Q^{0\prime}$	−1.3	1.9	2.9
	Q^0	−2.8	11.0	49.7
	Q^1	−13.3	10.4	37.9
	Q^2	−25.7	11.2	9.5
Stabilised glass (250 °C)	$Q^{0\prime}$	−1.4	1.0	0.3
	Q^0	−4.3	8.1	14.6
	Q^1	−13.5	11.0	41.9
	Q^2	−26.2	10.1	43.3
Stabilised glass (250 °C) (^{1}H–^{31}P CP)	Q^0	−3.6	6.4	21.2
	Q^1	−13.5	8.4	67.6
	Q^2	−25.8	9.9	11.2
Melt-quenched glass	Q^1	−7.9	7.4	5.0
	Q^2	−24.2	10.1	95.0

Table 2 Infrared band assignments[a] for the $(CaO)_{0.3}(Na_2O)_{0.2}$-$(P_2O_5)_{0.5}$ sol–gel and melt-quenched samples

Wavenumber/cm^{-1}	Assignment[b]	Associated Q^n (where applicable)
532	δ(P–O–P)	
725	ν_s(P–O–P)	
770	ν_s(P–O–P)	
900	ν_{as}(P–O–P)	Q^2
1000	$\nu_s(PO_3)^{2-}$	Q^1
1100	$\nu_{as}(PO_3)^{2-}$	Q^1
1270	$\nu_{as}(PO_2)^-$	Q^2
1640	$\delta(H_2O)$	
2970	ν(C–H)	
3430	ν(O–H)	

[a] Abbreviations: δ, deformation; ν, stretching; s, symmetric; as, asymmetric. [b] Refs. 22–25.

according to previous studies of phosphate-based glasses using infrared spectroscopy.[22–25] These assignments are listed in Table 2. Also included in Table 2, where applicable, is the Q^n species associated with each vibrational mode. The spectra from the sol–gel samples both exhibit the bands characteristic of P–O–P bonding at 532, ~750 and 900 cm^{-1} indicating that a significant number of these bonds are formed during the sol–gel reaction. Consistent with the ^{31}P NMR results, all the spectra contain bands exclusive to Q^1 and Q^2 groups: the presence of Q^1 units is characterised by the symmetric and asymmetric PO_3^{2-} stretching modes at 1000 and 1100 cm^{-1}, respectively, and the presence of Q^2 groups is evidenced by the asymmetric P–O–P and PO_2^- vibrations at 900 and 1270 cm^{-1}. The vibrations at about 2900 cm^{-1} in the spectra from the sol–gel samples are indicative of the presence of some residual organic material, whereas the bands at ~3400 and 1600 cm^{-1} are due to the presence of hydroxyl groups and adsorbed moisture. There are two regions of significant difference between the spectra from the sol–gel samples. Firstly, the intensity of the bands at 1600, 2900 and 3400 cm^{-1} is significantly reduced in the spectrum from the stabilised sol–gel glass, providing further evidence that residual organic components and hydroxyls are driven off during heat treatment. Consistent with the ^{31}P NMR data, the infrared spectrum from the stabilised sol–gel glass shows that although most of the organic material is removed by the heat treatment, a significant proportion of the hydroxyl groups remain. The second significant difference between the spectra shown in Fig. 5 is the relative intensities of the two pairs of Q^1- and Q^2-associated bands. In the spectrum from the dried gel, the intensity of the Q^2 peak at 1270 cm^{-1} is similar to that of the Q^1 peak at 1100 cm^{-1} and the intensity of the Q^1 peak at 1000 cm^{-1} is only slightly less that of the Q^2 peak at 900 cm^{-1}. After heat treatment, the Q^2 band at 1270 cm^{-1} is significantly more intense than the Q^1 peak at 1100 cm^{-1}. A similar change is observed for the other pair of bands with the Q^2 peak at 900 cm^{-1} growing in intensity relative to the Q^1 peak at 1000 cm^{-1}. This latter difference suggests, in agreement with the ^{31}P NMR measurements, an increase in the proportion of Q^2 structural units with heat treatment. The spectrum from the melt-quenched sample is similar to that from the sol–gel sample, although there are some significant differences. Notably, the relative intensity of the Q^2 band at 1270 cm^{-1}

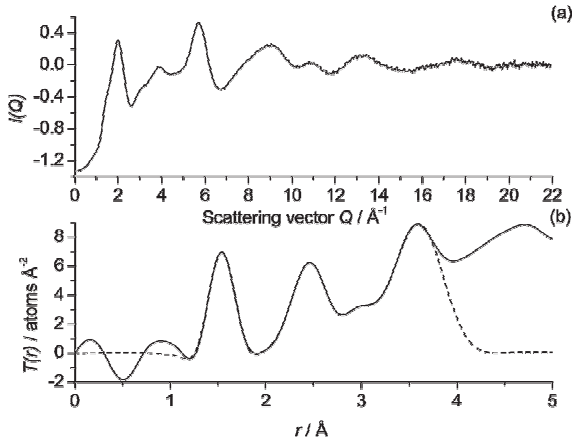

Fig. 6 X-Ray diffraction data from the $(CaO)_{0.3}(Na_2O)_{0.2}(P_2O_5)_{0.5}$ sol–gel dried at 120 °C: (a) Q-space interference function, $i(Q)$, and (b) pair-distribution function, $T(r)$, (solid line) together with fit (dashed line).

compared to the Q^1 band at 1100 cm^{-1} is greater for the melt-quenched glass. Also the ν_s(P–O–P) bands at ~750 cm^{-1} are more intense for the melt-quenched glass. Both these differences suggest greater connectivity between the PO_4^{3-} structural units in the melt-quenched glass compared to the sol–gel glass. Finally, the bands associated with hydroxyl groups are very weak, but nonetheless observable, in the spectrum from the melt-quenched glass. This suggests partial hydrolysis of the network structure, probably by atmospheric moisture, and is consistent with the presence of a small proportion of Q^1 units, as observed with ^{31}P NMR.

The HEXRD measurements give information on the pair-wise correlations between atoms within a material. Fig. 6 and 7 show the HEXRD data from the $(CaO)_{0.3}(Na_2O)_{0.2}(P_2O_5)_{0.5}$ sol–gel sample, both prior to and after heat treatment. Both the r-space and Q-space data are shown, together with the fits to the pair-distribution functions obtained using the method described above. Fig. 8 shows the equivalent curves measured from the analogous melt-quenched glass for comparison. The

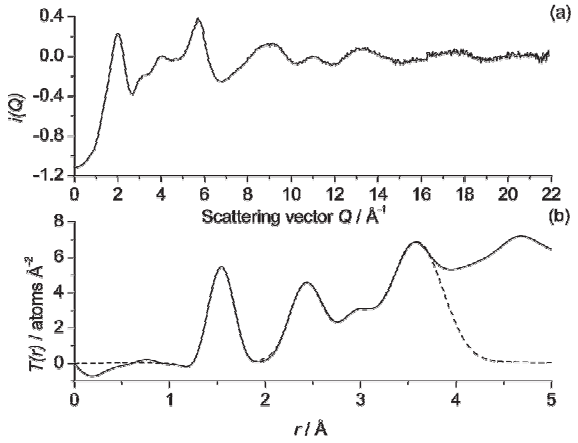

Fig. 7 X-Ray diffraction data from the $(CaO)_{0.3}(Na_2O)_{0.2}(P_2O_5)_{0.5}$ sol–gel heat treated to 250 °C: (a) Q-space interference function, $i(Q)$, and (b) pair-distribution function, $T(r)$, (solid line) together with fit (dashed line).

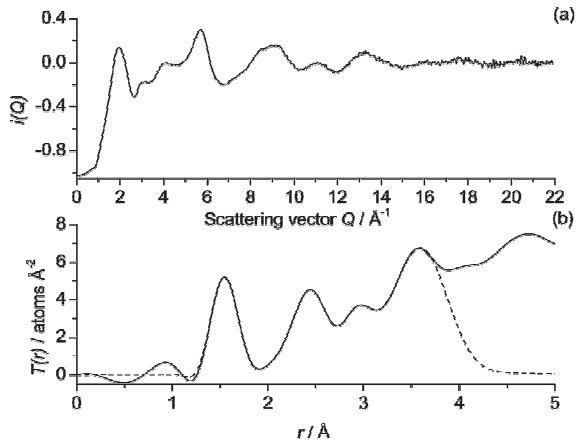

Fig. 8 X-Ray diffraction data from the $(CaO)_{0.3}(Na_2O)_{0.2}(P_2O_5)_{0.5}$ melt-quenched glass: (a) Q-space interference function, $i(Q)$, and (b) pair-distribution function, $T(r)$, (solid line) together with fit (dashed line).

structural parameters obtained from the fitting of the HEXRD data are given in Table 3.

All three pair-distribution functions follow a similar profile with features at around 1.5, 2.5 and 3.0 Å. These features are characteristic of phosphate-based structures that have at least some connectivity between PO_4^{3-} tetrahedra.[19] The peak at 1.5 Å is due to P–O bonding within the PO_4^{3-} tetrahedron. It is well known that phosphate-based glasses contain two P–O distances: a shorter distance of 1.43 to 1.52 Å ascribed to P–NBO bonds and a longer distance of 1.58 to 1.63 Å due to P–BO bonds.[19,26] In this case, we have simulated the $T(r)$ functions with two P–O distances. The results in Table 3 show that for all three samples the measured P–O distances are consistent with those from previous structural studies of similar materials[19,20,26] and that the total P–O coordination number is close to four with approximately equal number of P–NBO and P–BO bonds, as expected for glassy materials close to the metaphosphate composition. The peak at around 2.5 Å has contributions from both nearest-neighbour O···O distances within PO_4^{3-} tetrahedra and from distances between oxygen atoms in adjacent connected phosphate groups. The structural parameters obtained for this O···O correlation in Table 3 are similar for all three samples. The third feature at around 3 Å can be ascribed to the P···P distance between the phosphorus atoms of PO_4^{3-} tetrahedra which are connected by a bridging oxygen atom.

The coordination number associated with this P···P nearest-neighbour distance displays the most variation between samples. The melt-quenched glass has a $N_{P...P}$ of 2.1 ± 0.2 which is very close to the expected value of two for a material at the metaphosphate composition with a structure composed of Q^2 phosphate units and shows excellent agreement with the value calculated from the ^{31}P NMR results. The sol–gel glass has a $N_{P...P}$ of 1.5 ± 0.2, whereas the value for the dried gel is 1.1 ± 0.3. The reduction in $N_{P...P}$ for the sol–gel samples is consistent with the presence of a significant proportion of Q^0 and Q^1 units in the structure as determined by ^{31}P NMR. The HEXRD $N_{P...P}$ values for the sol–gel samples agree with those from the NMR work if one takes into account the experimental errors, which largely result from the fitting processes used to simulate the data. The discrepancy in P···P coordination numbers determined for the dried gel (0.6 from NMR and 1.1 from HEXRD) reflects the difficulty in fitting the data from this sample: in the HEXRD $T(r)$ function, the P···P correlation is weak and not well-resolved from adjacent peaks, and the Q^0 and Q^1 contributions to the ^{31}P NMR spectrum are also not clearly resolved. The $N_{P...P}$ of ~1 obtained from the HEXRD data seems more reasonable since this represents a significant degree of polymerisation necessary for gelation. The increase in $N_{P...P}$ with heat treatment represents consolidation of the sol–gel structure as hydroxyl and unreacted alkoxide groups are driven off. The value of 1.5 for $N_{P...P}$ in the heat-treated sol–gel glass is still significantly lower than that of 2.1 measured for the melt-quenched glass due to the reduced network connectivity associated with the presence of hydroxyl groups as evidenced by the infrared and ^1H–^{31}P CP

Table 3 Structural parameters obtained from the simulation of the HEXRD data from the $(CaO)_{0.3}(Na_2O)_{0.2}(P_2O_5)$ samples

Sample	Density/atoms Å^{-3}	Correlation	R/Å	N	σ/Å
Dried sol–gel (120 °C)	0.0861	P–NBO	1.50(1)	2.0(1)	0.02(1)
		P–BO	1.59(1)	1.9(1)	0.05(1)
		Na–O	2.32(2)	3.9(5)	0.12(2)
		Ca–O	2.38(2)	4.9(5)	0.07(2)
		O···O	2.54(2)	4.4(2)	0.08(1)
		P···P	2.96(2)	1.1(3)	0.07(2)
		O···O_{2nd}	2.82(2)	1.0(4)	0.11(3)
Sol–gel glass (250 °C)	0.0694	P–NBO	1.50(1)	1.8(1)	0.02(1)
		P–BO	1.59(1)	1.8(1)	0.04(1)
		Na–O	2.34(2)	3.0(5)	0.10(2)
		Ca–O	2.37(2)	4.6(5)	0.05(2)
		O···O	2.54(2)	4.0(2)	0.08(1)
		P···P	2.96(2)	1.5(2)	0.08(2)
		O···O_{2nd}	2.81(2)	1.2(4)	0.12(3)
Melt-quenched glass	0.0726	P–NBO	1.50(1)	1.8(1)	0.02(1)
		P–BO	1.60(1)	1.9(1)	0.05(1)
		Na–O	2.33(2)	4.5(5)	0.11(2)
		Ca–O	2.38(2)	5.2(5)	0.11(2)
		O···O	2.52(1)	4.1(2)	0.08(1)
		P···P	2.94(2)	2.1(2)	0.08(2)
		O···O_{2nd}	2.81(2)	1.8(4)	0.13(3)

NMR spectra. The fact that the changes in $N_{P\cdots P}$ are not reflected in changes in the numbers of P–BO and P–NBO bonds as would be expected with a changing Q^n distribution is due to the difficulty in separating the two overlapping contributions to the P–O peak at 1.5 Å.

The contribution to the $T(r)$ functions from the Na–O and Ca–O correlations appears as a shoulder on the low-r side of the main O···O peak. The results in Table 3 concerning the coordination spheres of the sodium and calcium cations are similar for all three samples. Furthermore, these parameters are consistent with those previously measured from $(CaO)_{0.5-x}(Na_2O)_x(P_2O_5)_{0.5}$ binary and ternary glasses using neutron diffraction.[20]

To summarize the results of the structural study, we can say that the sol–gel synthesis and processing (*i.e.* low temperature heat treatment) produces a glassy material with a similar structure to that of its melt-quenched counterpart. The important difference is that the structure of the sol–gel glass contains a significant fraction of hydroxyls which act as phosphate-chain terminating groups leading to a reduced connectivity of the network structure.

Conclusions

We have presented a new method for the sol–gel synthesis of $CaO–Na_2O–P_2O_5$ glass with potential application in the field of biomaterials. Thermal analysis and high-temperature XRD characterisation of the dried gel demonstrated that consolidation of the structure and removal of residual organic fragments starts occurring above 200 °C and that the material remains amorphous up to ~470 °C. The structural characterisation of the heat-treated sample revealed that it comprises Q^1 and Q^2 phosphate units with a significant concentration of hydroxyls which act as phosphate-chain terminating groups. Comparison of the structure with that of the melt-quenched analogue shows that the structures of the two materials are very similar except for the presence of a significant proportion of hydroxyl groups in the sol–gel material. This demonstrates that glassy $CaO–Na_2O–P_2O_5$ materials can be prepared at 'oven' temperatures rather than 'furnace' temperatures and allows scope for the preparation of inorganic/polymer composite materials and 3D scaffolds for tissue engineering applications.

Acknowledgements

The authors wish to acknowledge funding from the EPSRC (EP/C000714, EP/C000633 and GR/T21080). We thank Mark Roberts of the CCLRC Daresbury Laboratory for his assistance in the use of station 9.1.

References

1 J. C. Knowles, *J. Mater. Chem.*, 2003, **13**, 2395–2401.
2 A. Kesisoglou, J. C. Knowles and I. Olsen, *Key Eng. Mater.*, 2005, **284**, 597–600.
3 I. Ahmed, C. A. Collins, M. P. Lewis, I. Olsen and J. C. Knowles, *Biomaterials*, 2004, **25**, 3223–3232.
4 M. Bitar, J. C. Knowles, M. P. Lewis and V. Salih, *J. Mater. Sci.: Mater. Med.*, 2005, **16**, 1131–1136.
5 A. M. Mulligan, M. Wilson and J. C. Knowles, *J. Biomed. Mater. Res., Part A*, 2003, **67**, 401–412.
6 I. Ahmed, D. Ready, M. Wilson and J. C. Knowles, *J. Biomed. Mater. Res., Part A*, 2006, **79**, 618–626.
7 T. Gilchrist, M. A. Glasby, D. M. Healy, G. Kelly, D. V. Lenihan, K. L. McDowall, I. A. Miller and L. M. Myles, *Br. J. Plast. Surg.*, 1998, **51**, 231–237.
8 D. V. Lenihan, A. J. Carter, T. Gilchrist, D. M. Healy, L. M. Miller and M. A. Glasby, *J. Hand Surg.–Br. Eur. Vol.*, 1998, **23B**, 588–593.
9 K. J. Toumba and M. E. J. Curzon, *J. Dent. Res.*, 1997, **76**, 964–964.
10 K. J. Toumba and M. E. J. Curzon, *J. Dent. Res.*, 1997, **76**, 1041–1041.
11 J. Livage, P. Barboux, M. T. Vandenborre, C. Schmutz and F. Taulelle, *J. Non-Cryst. Solids*, 1992, **147**, 18–23.
12 D. Carta, D. M. Pickup, J. C. Knowles, M. E. Smith and R. J. Newport, *J. Mater. Chem.*, 2005, **15**, 2134–2140.
13 I. Ahmed, M. Lewis, I. Olsen and J. C. Knowles, *Biomaterials*, 2004, **25**, 501–507.
14 E. A. Abou Neel, I. Ahmed, J. Pratten, S. N. Nazhat and J. C. Knowles, *Biomaterials*, 2005, **26**, 2247–2254.
15 J. M. Cole, E. R. H. van Eck, G. Mountjoy, R. Anderson, T. Brennan, G. Bushnell-Wye, R. J. Newport and G. A. Saunders, *J. Phys.: Condens. Matter*, 2001, **13**, 4105–4122.
16 X. Qiu, J. W. Thompson and S. J. L. Billinge, *J. Appl. Crystallogr.*, 2004, **37**, 678.
17 P. H. Gaskell, *Materials Science and Technology*, VCH, Weinheim, 1991.
18 P. N. Gunawidjaja, M. A. Holland, G. Mountjoy, D. M. Pickup, R. J. Newport and M. E. Smith, *Solid State Nucl. Magn. Reson.*, 2003, **23**, 88–106.
19 R. K. Brow, *J. Non-Cryst. Solids*, 2000, **263**, 1–28.
20 D. M. Pickup, I. Ahmed, P. Guerry, J. C. Knowles, M. E. Smith and R. J. Newport, *J. Phys.: Condens. Matter*, 2007, in press.
21 A. F. Ali, P. Mustarelli, E. Quartarone and A. Magistris, *J. Mater. Res.*, 1999, **14**, 327–329.
22 L. Baia, D. Muresan, M. Baia, J. Popp and S. Simon, *Vib. Spectrosc.*, 2007, **43**, 313–318.
23 D. Ilieva, B. Jivov, G. Bogachev, C. Petkov, I. Penkov and Y. Dimitriev, *J. Non-Cryst. Solids*, 2001, **283**, 195–202.
24 Y. M. Moustafa and K. El-Egili, *J. Non-Cryst. Solids*, 1998, **240**, 144–153.
25 J. O. Byun, B. H. Kim, K. S. Hong, H. J. Jung, S. W. Lee and A. A. Izyneev, *J. Non-Cryst. Solids*, 1995, **190**, 288–295.
26 A. C. Hannon, *Nucl. Instrum. Methods Phys. Res., Sect. A*, 2005, **551**, 88–107.